IEEE Access
Multidisciplinary ⋮ Rapid Review ⋮ Open Access Journal

Received September 4, 2021, accepted September 23, 2021, date of publication September 29, 2021,
date of current version October 7, 2021.

Digital Object Identifier 10.1109/ACCESS.2021.3116714

Low-Profile Wideband Unidirectional Circularly Polarized Metasurface-Based Bowtie Slot Antenna

CHO HILARY SCOTT NKIMBENG, HEESU WANG, (Graduate Student Member, IEEE), AND IKMO PARK, (Member, IEEE)

Department of Electrical and Computer Engineering, Ajou University, Suwon-si 16499, Republic of Korea

Corresponding author: Ikmo Park (ipark@ajou.ac.kr)

This work was supported in part by the National Research Foundation (NRF) of Korea funded by the Korean Government [Ministry of Science and ICT (MSIT)] under Grant 2018R1D1A1A02086071, and in part by the Gyeonggi Regional Research Center (GRRC) Program of Gyeonggi Province under Grant GRRC AJOU 2016B01 (Photonics-Medical Convergence Technology Research Center).

ABSTRACT In this paper, the design of a wideband circularly polarized (CP) bowtie slot antenna that uses metasurfaces is presented. The antenna consists of a single-layer substrate with the metasurface made of 4 × 4 periodic corner-truncated patches printed at the top side of the substrate and a bowtie-shaped slot etched on the ground plane. The metasurface made of corner-truncated patches are utilized to convert the linearly polarized wave into a CP wave. The antenna is fed by a 50-Ω coplanar waveguide. The antenna, with an overall size of 42 mm × 42 mm × 2.3 mm (0.71 λ_o × 0.71 λ_o × 0.038 λ_o at 5.1 GHz), was fabricated and measured. The measured reflection coefficient for $|S_{11}| < -10$ dB yielded an impedance bandwidth of 3.75–6.67 GHz (55.7%), an axial ratio (AR) bandwidth of 4.38–5.98 GHz (31.37%), a 3-dB gain bandwidth of 3.75–6.0 GHz (46.88%), a peak gain of 7 dBic, and a high radiation efficiency of more than 93% within the AR bandwidth.

INDEX TERMS Bowtie slot, circular polarization, low-profile, metasurface, slot antenna.

I. INTRODUCTION

In recent years, metamaterials have attracted considerable attention and have been applied to antennas to enhance performance due to their unique abilities to manipulate and produce electromagnetic waves that are unusual or difficult to obtain in nature [1]–[3]. As a subfield of metamaterials, metasurfaces have been widely used to realize low-profile broadband antennas [4]–[12] and circularly polarized (CP) antennas [13]–[28]. Recently, CP antennas have become an attractive source for many satellite and wireless communication applications owing to their advantage of flexibility in transmitter/receiver orientations for stable and reliable signal transmission and reception [26]–[29]. Nowadays, many planar two-dimensional metamaterial (metasurface) polarizers have been designed to realize CP waves from linear polarized (LP) waves [30]–[32]. Metasurfaces have been extensively employed in applications involving antennas to improve antenna performance, such as the enhancement of bandwidth, increase in radiation gain, and size reduction for various types of antennas.

Recently, various linear-to-circular wave conversion structures have been investigated in metasurface CP antenna design [15]–[21]. In [15], the authors used 16 unit cells in a 4 × 4 metasurface layout, with each unit cell having a rectangular loop with a diagonal microstrip for LP to CP wave conversion. However, the antenna had poor mechanical properties due to the use of an air layer that separated the source antenna and the metasurface. The authors in [16] proposed a corner-truncated reconfigurable metasurface antenna without an air gap. Even though the antenna was compact, its AR bandwidth was narrow. In [17], a miniaturized antenna using capacitive loading strips on a corner-truncated patch was investigated. A pair of capacitive loading strips was inserted along the diagonal of a corner-truncated patch to achieve an antenna size reduction of more than 50%. However, both the impedance bandwidth and AR bandwidth were limited. In [18], the authors proposed a metasurface structure consisting of four unit cells with parasitic square cross-gaps arranged in a 2 × 2 layout for LP to CP polarization conversion.

The associate editor coordinating the review of this manuscript and approving it for publication was Diego Masotti.

They achieved a low profile and wide impedance bandwidth (39.35%), yet the AR bandwidth (17.7%) was narrow. In [19], another compact metasurface antenna, consisting of 4 × 4 ellipse patches with a 45° rotation, was used for the conversion of LP to CP waves. Although a wide impedance bandwidth of 20.6% was achieved, a limited AR bandwidth was obtained, similar to that reported in [18]. Thus, the simultaneous enhancement of AR bandwidth and reduction in antenna size is still challenging, and many studies are being conducted to address these issues. Some researchers have proposed techniques to improve AR bandwidth and impedance bandwidth using different types of metasurface patches, but they use extremely thick substrates [20], [21]. In [20], a CP slot antenna was proposed using a corner-truncated metasurface for polarization conversion. An S-shaped metasurface polarization converter for LP to CP wave conversion was presented in [21]. Both antennas achieved wide impedance and AR bandwidths. However, the use of an extremely thick substrate increases the volume of the antenna, rendering it bulky and limiting its practical applications. Slot antennas have numerous fascinating advantages over microstrip antennas, as they provide wider bandwidths, good impedance matching, lower radiation loss, and the possibility of obtaining bidirectional radiation patterns [33]–[35]. A prominent way of increasing the bandwidth of a slot antenna is by increasing the width of a rectangular slot [36] or a bowtie slot [37], [38]. In all previous works, with polarization converters using slot antennas as an LP source [16]–[21], the authors employed narrow-width slot antennas. Even though they employed wideband circularly polarized metasurface patches, they obtained narrow impedance and AR bandwidths. This paper proposes a novel method of achieving wide impedance and AR bandwidths by using a modified bowtie wide slot antenna and coupling it with a conventional wideband LP-to-CP polarization converter.

This paper presents a low-profile wideband CP stepped bowtie slot antenna that uses the metasurface made of corner-truncated patches for the polarization conversion from an LP wave to a CP wave. The antenna consists of the metasurface made of 4 × 4 corner-truncated patches placed at the top of the antenna and a bowtie-shaped wide slot placed at the bottom of the antenna. The resulting antenna shows good performance characteristics with a wide impedance bandwidth of 3.75–6.67 GHz (55.7%), a wideband AR bandwidth of 4.38–5.98 GHz (31.37%), a 3-dB gain bandwidth of 3.75–6.0 GHz (46.88%), a peak gain of 7 dBic, and a radiation efficiency greater than 93% within the AR bandwidth. The antenna dimensions are 42 mm × 42 mm × 2.3 mm (0.71 λ_o × 0.71 λ_o × 0.038 λ_o at 5.1 GHz).

II. ANTENNA GEOMETRY AND DESIGN

The geometry of the proposed antenna is shown in Fig. 1. The antenna consists of a single layer RO4003 (ε_r = 3.38, tanδ = 0.0027) dielectric substrate in the dimensions 42 × 42 × 2.3 mm^3. The metasurface is printed on top

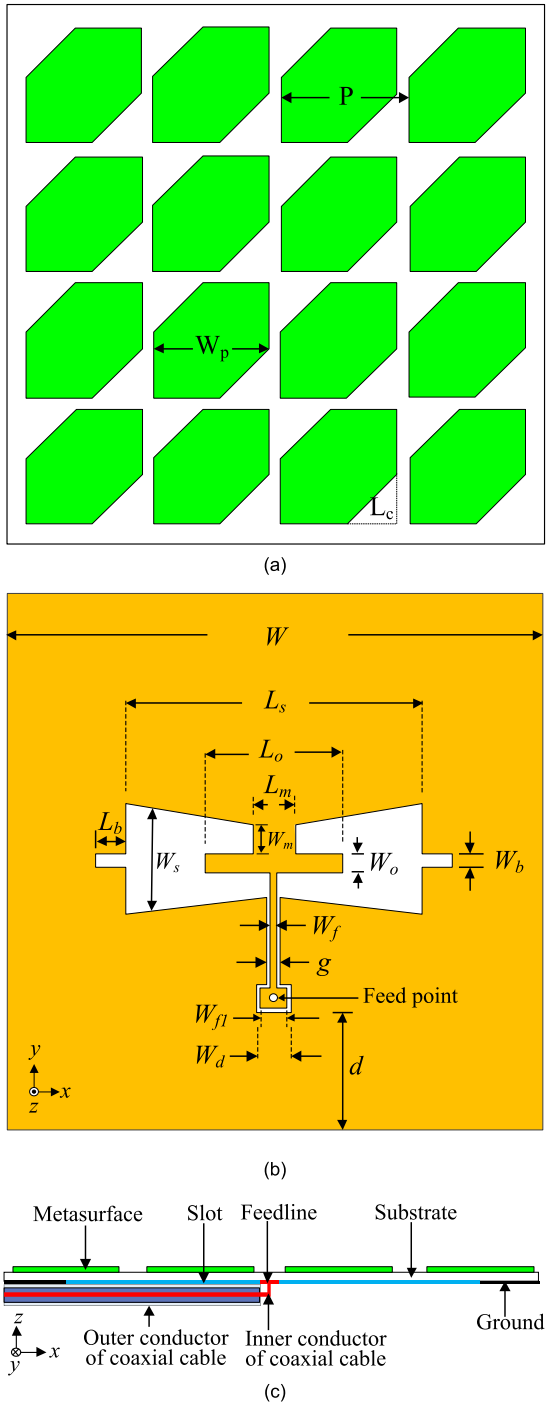

FIGURE 1. (a) Corner-truncated 4 × 4 patches, (b) slot etched on the ground plane, and (c) side view.

of the substrate, and the stepped bowtie slot is etched on the ground plane on the bottom of the substrate. The metasurface is a periodic structure with 16 square metal plates arranged in a 4 × 4 layout with periodicity P. A truncation with dimensions of L_c is created on the patches with a size of W_p × W_p to produce CP radiation, as shown in Fig. 1(a). The primary radiating element of the antenna is the slot, as shown in Fig. 1(b). It consists of an inner bowtie slot with

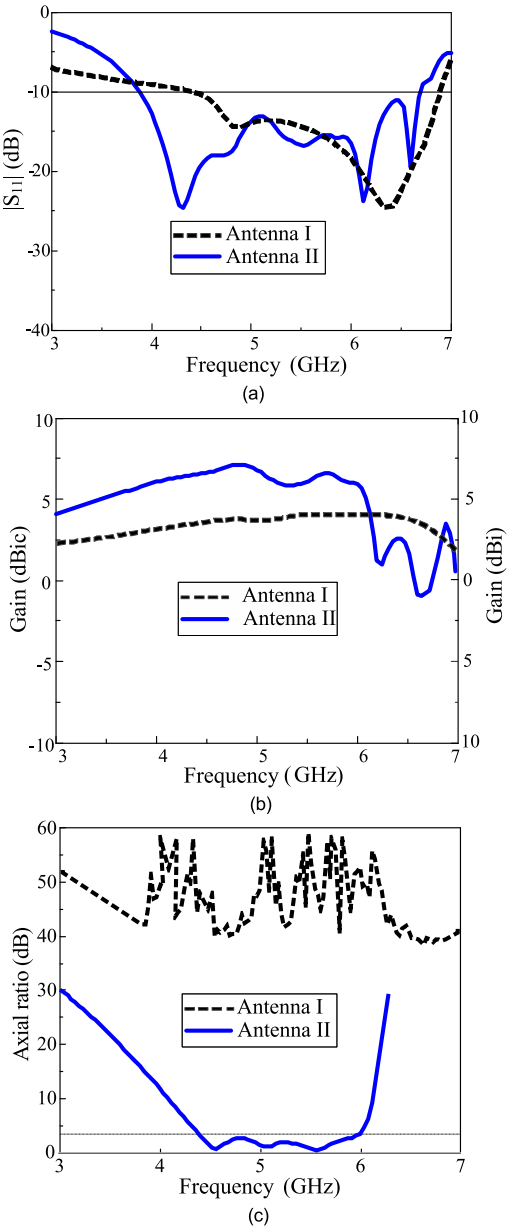

FIGURE 2. (a) Reflection coefficient, (b) gain, and (c) AR of antenna I and antenna II.

slot length L_s and width W_s, which determine the resonance frequency of the antenna, and two small identical rectangular slots with length L_b and width W_b attached to both edges of the bowtie slot to provide impedance matching and good AR of the antenna. The two stubs of lengths L_m and L_o are used for the impedance matching of the antenna. Excitation is provided by the 50-Ω coplanar waveguide (CPW), which is printed on the bottom of the antenna structure, as shown in Fig. 1(c). As shown in Fig. 1(b), the feeding position of the CPW is moved by a distance d along the y-axis direction, and a coaxial-to-coplanar transition [32], [33] of widths W_{f1} and W_d is made to connect the coaxial inner conductor perpendicularly to the CPW center conductor. With the coaxial-to-coplanar transition, the radial electric field of

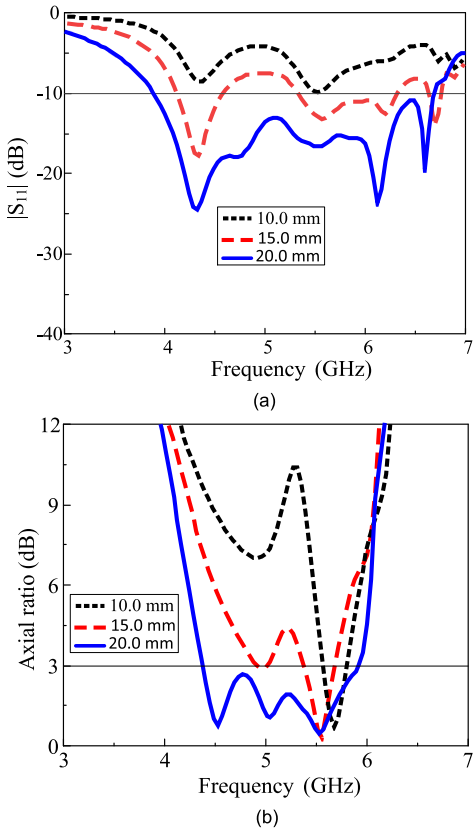

FIGURE 3. Effect of inner slot length (L_s): (a) reflection coefficient and (b) axial ratio.

the coaxial cable directly couples on the same plane with the electric field in the gap of the CPW [32], [39]. This feeding configuration poses significant advantages over the conventional method of CPW feeding [25], [40], [41] that connects the coaxial inner conductor and the CPW center. The SMA inner conductor is connected perpendicularly to the CPW center conductor, while the SMA outer conductor is connected to the ground plane. To ease the fabrication of the antenna, the inner conductor of the SMA was bent a little to connect with the center conductor of the CPW, as shown in Fig. 11(b), and the outer conductor connected to the ground plane and then bent to the edge of the antenna to make it firm for antenna measurement. Using the Ansoft High-Frequency Structure Simulator (HFSS), which is an electromagnetic wave simulator using a finite element method, the antenna is determined to achieve low-profile broadband impedance matching and wideband CP radiation. The optimized design parameters of the antenna are as follows: $P = 10.2$ mm, $W_p = 10.1$ mm, $L_c = 4$ mm, $g = 0.1$ mm, $W_f = 0.4$ mm, $L_s = 20$ mm, $W_s = 8.3$ mm, $W_d = 1.2$ mm, $W_{f1} = 0.8$ mm, $L_m = 3$ mm, $L_o = 9.2$ mm, $W_o = 2$ mm, $W_m = 2.4$ mm, $L_b = 2$ mm, $W_b = 1$ mm, d = 10.1 mm, $W = 42$ mm, and $h = 2.3$ mm.

The design guidance and methodology of the proposed antenna were:

1. The antenna was designed using a conventional bowtie slot structure with symmetric flare angles to operate at

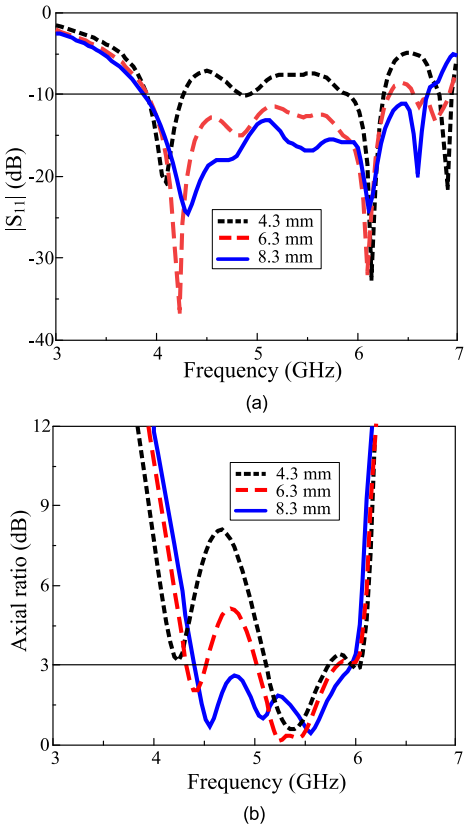

FIGURE 4. Effect of inner slot width (W_s): (a) reflection coefficient and (b) axial ratio.

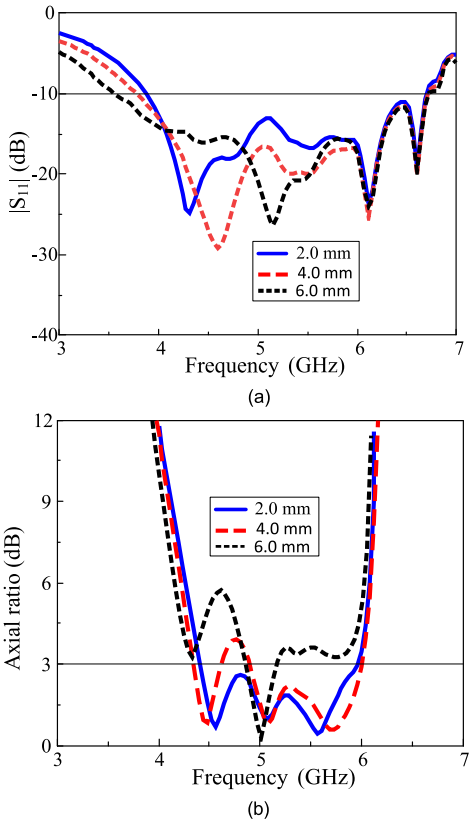

FIGURE 5. Effect of outer slot length (L_b): (a) reflection coefficient and (b) axial ratio.

the desired frequency. The antenna consists of an inner bowtie slot (L_s, W_s), which determines the resonant frequency. The slot length (L_s) is about half the effective wavelength at the operating frequency. For the antenna feeding, a coaxial-to-coplanar transition of widths W_{f1} and W_d is performed.

2. The bowtie slot was modified by introducing two identical rectangular slots at both edges to provide good impedance matching and AR. Two stubs were also employed to further provide good impedance matching.

3. Design the unit cell of the metasurface (P, W_p, L_c) over the target operating frequency band.

4. The antenna with the unidirectional radiation pattern is obtained by stacking the metasurface layer above the radiator. Finally, the antenna parameters of both the bowtie wide slot antenna and the corner-truncated metasurface patch are adjusted for wide impedance and AR bandwidths.

For a better understanding of the operational mechanism of the proposed antenna, the stepped bowtie-shaped slot antenna structure is simulated without the metasurface (Antenna I), and its antenna characteristics are compared with those of the proposed stepped bowtie-shaped slot coupled with the metasurface made of 4 × 4 corner-truncated patches (Antenna II). The simulated results for $|S_{11}|$, the gain, and the AR for Antenna I and Antenna II are shown in Fig. 2. Antenna I achieves an impedance bandwidth of 38.9%, which covers 4.7 to 7 GHz, as shown in Fig. 2(a), a peak gain of 4.3 dBi, as shown in Fig. 2 (b), and an AR > 40 dB, as shown in Fig. 2(c). By introducing a metasurface composed of 4 × 4 corner-truncated square patches, Antenna II achieves a wide impedance bandwidth of 56.7%, which covers 3.75 to 6.7 GHz, as shown in Fig. 2(a), a peak gain of 7.2 dBic, and a wide 3-dB AR bandwidth of 31.76% (4.36–5.98 GHz), as shown in Figs. 2(b) and 2(c), respectively. Antenna I (slot only) produces bidirectional radiation where almost half of the power is radiated in the backward direction, which leads to low directivity in the forward direction and limits its applications. The introduction of metasurface (Antenna II) above Antenna I improves the front-to-back ratio by reducing the backward radiation (–z-axis) and enhancing the gain at the broadside (+z-axis) due to the strong coupling of the slot to the metasurface causes the antenna to radiate more power in the broadside direction. At 5.1 GHz, the front-to-back ratio is 0.4 dB without the metasurface whereas the front-to-back ratio is 10.9 dB with the metasurface. The right-hand (RH) CP is dominant over the left-hand (LH) CP fields, and unidirectional radiation is achieved. The impedance bandwidth of Antenna II is wider compared with that of Antenna I, as shown in Fig. 2(a), because the metasurface in Antenna II creates additional resonance, which increases the impedance bandwidth. As shown in Fig. 2(c), Antenna I is linearly polarized, as its AR is greater than 40 dB; however, Antenna II

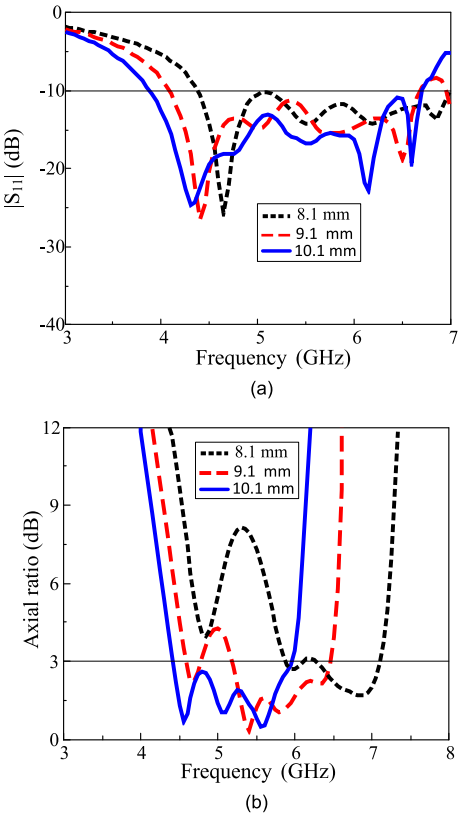

FIGURE 6. Effect of patch size (W_p): (a) reflection coefficient and (b) axial ratio.

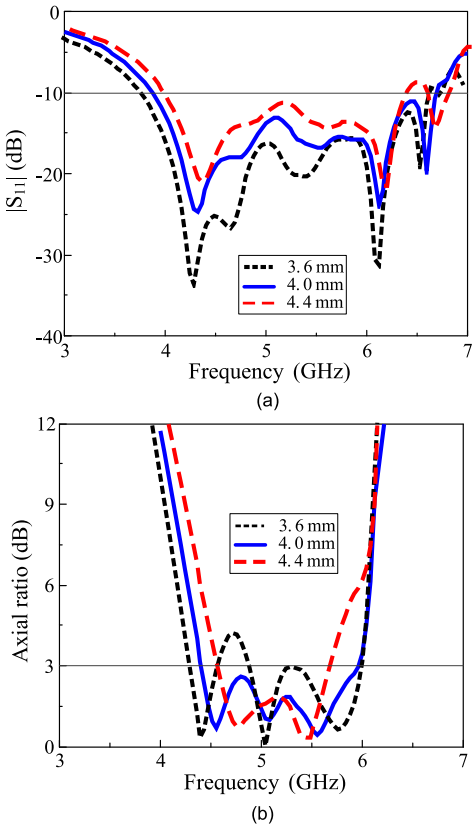

FIGURE 7. Effect of cut size (L_c): (a) reflection coefficient and (b) axial ratio.

produces CP waves with an AR of less than 3 dB that covers 4.36–5.98 GHz. CP radiation is achieved in Antenna II due to the presence of the corner-truncated metasurface that converts the LP wave produced by Antenna I into a CP wave. The mechanism of CP generation and unit cell analysis of the corner-truncated metasurface patch has been investigated in [20] and [42]–[44]. The E-field ($\mathbf{E}$) produced by Antenna I is resolved into two orthogonal components ($\mathbf{E}_1$ and $\mathbf{E}_2$) when it interacts with the corner-truncated metasurface in Antenna II. Wideband CP radiation is obtained by adjusting the parameters of the metasurface to obtain $|E_1| = |E_2|$ and $\angle(E_1–E_2) = 90°$.

III. PARAMETRIC STUDY

The simulation and optimization of the proposed antenna were performed using an Ansys HFSS. The effects of crucial antenna parameters on antenna characteristics were investigated. First, the response of the antenna was determined when all the parameters were fixed at their optimal values. Second, one design parameter at a time was varied during the parametric study. The key antenna parameters included the inner slot length (L_s), inner slot width (W_s), outer slot length (L_b), patch size (W_p), cut size (L_c), feedline width (W_f), and stub length (L_m). The simulated reflection coefficient and AR of the optimized antenna with the design parameters given in Section II are presented in Figs. 12 and 14, respectively. The antenna exhibits an $|S_{11}| < -10$ dB, an impedance bandwidth of 56.7% covering 3.75–6.7 GHz, and an AR bandwidth of 31.76% covering 4.36–5.98 GHz.

The effect of varying the inner slot length (L_s) on the reflection coefficient and AR is shown in Figs. 3(a) and (b), respectively. As the inner slot length increases from 10 mm to 20 mm, the resonance shifts to lower frequencies, as shown in Fig. 3(a). As shown in Fig. 3(b), as the inner slot length increases from 10 mm to 20 mm, the AR bandwidth moves to lower frequencies. The effect of varying the inner slot width on the reflection coefficient and AR is shown in Figs. 4(a) and (b), respectively. As shown in Fig. 4(a), as the inner slot width (W_s) increases from 4.3 mm to 8.3 mm, the resonance also shifts to lower frequencies. An increase in the inner slot width (W_s) lowers the AR, as shown in Fig. 4(b). The effect of varying the outer slot length (L_b) on the reflection coefficient and AR is shown in Figs. 5(a) and (b), respectively. As shown in Fig. 6(a), as the outer slot length (L_b) increases from 2 mm to 6 mm, there is a slight shift in the resonance frequency towards lower frequencies, and the antenna is better matched. Additionally, as the outer slot length (L_b) decreases from 6 mm to 2 mm, the AR is lowered, as shown in Fig. 5(b). The effect of varying the metasurface patch size (W_p) on the reflection coefficient and AR is shown in Figs. 6(a) and (b), respectively. As shown in Fig. 6(a), as the metasurface patch size (W_p) increases from 8.1 mm to 10.1 mm, there is a shift in the resonance frequency towards lower frequencies.

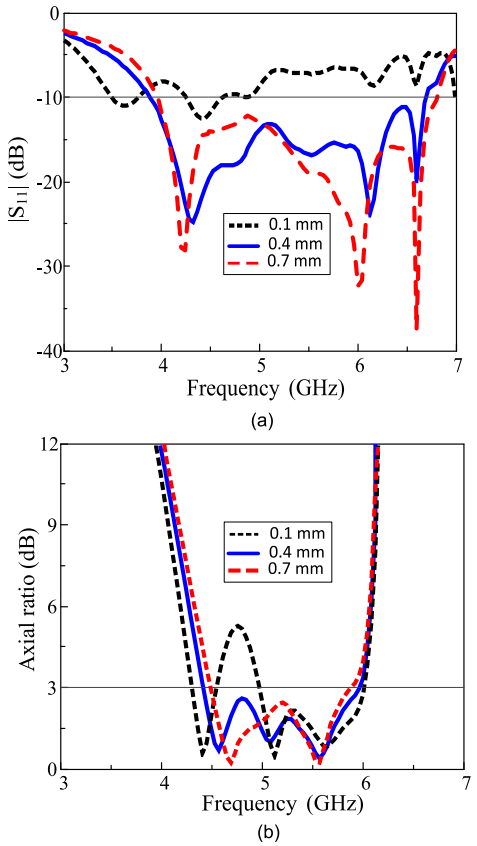

FIGURE 8. Effect of feedline (W_f): (a) reflection coefficient and (b) axial ratio.

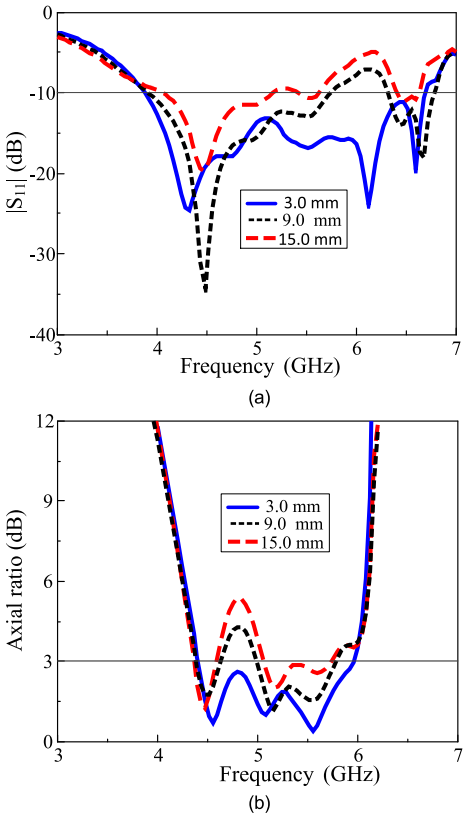

FIGURE 9. Effect of stub length (L_m): (a) reflection coefficient and (b) axial ratio.

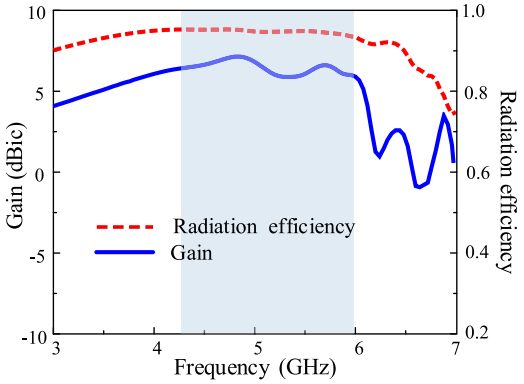

FIGURE 10. Gain and radiation efficiency.

Similarly, as shown in Fig. 6(b), an increase in the metasurface patch size (W_p) from 8.1 mm to 10.1 mm shifts the AR bandwidth to lower frequencies. An increase in the metasurface patch size leads to an increase in the overall size of the radiator and, thus, a shift in the resonance to lower frequencies. This phenomenon corresponds to resonant theory, in which resonance is inversely proportional to radiator size. The effect of varying the metasurface cut size (L_c) on the reflection coefficient and AR is shown in Figs. 7 (a) and (b), respectively. An increase in the metasurface cut size leads to a decrease in the metasurface patch size, and a decrease in the metasurface cut size leads to an increase in the metasurface patch size. Thus, when the cut size increases from 3.6 mm to 4.4 mm, there is a slight shift in the resonance frequency to a higher frequency due to the decrease in the metasurface patch. When the corner cut size L_c is increased from 3.6 mm to 4.0 mm, AR is lowered and well matched with AR $<$ 3 dB, as shown in Fig. 7(b); however, increasing L_c also leads to a decrease in the AR bandwidth. The effect of varying the feedline width (W_f) on the impedance and AR is shown in Figs. 8(a) and (b); when the feedline width $W_f = 0.1$ mm, the impedance of the antenna is not fully matched. As W_f increases to 0.4 mm and 0.7 mm, the resonance frequency decreases, good impedance matching is obtained, and a wide impedance bandwidth is achieved. An increase in the feedline width (W_f) lowers the AR, as shown in Fig. 8(b).

The effect of varying the stub length L_m on the impedance and AR is shown in Figs. 9(a) and (b). Decreasing L_m from 15.0 mm to 3.0 mm lowers the impedance of the antenna. At $L_m = 3.0$ mm, the impedance is well matched. Similarly, as shown in Fig. 9(b), decreasing the stub length (L_m) lowers the AR. The gain of the antenna and its radiation efficiency are presented in Fig. 10. The antenna exhibits stable gain characteristics with a peak gain of 7.15 dBic at the broadside direction for (phi $= 0°$) and (theta $= 0°$) and shows a high radiation efficiency of more than 93% within the AR bandwidth. The simulated radiation patterns in the

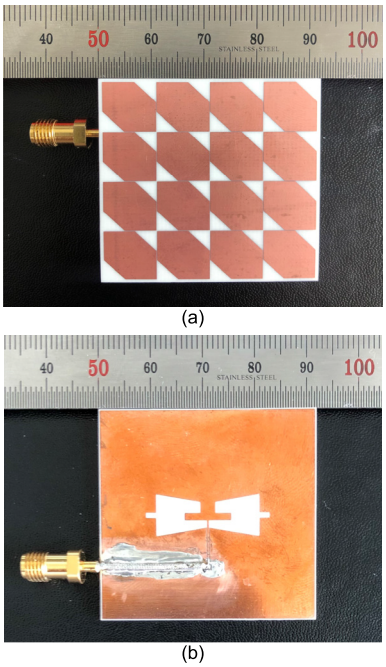

FIGURE 11. Fabricated sample of the proposed antenna: (a) top view and (b) bottom view.

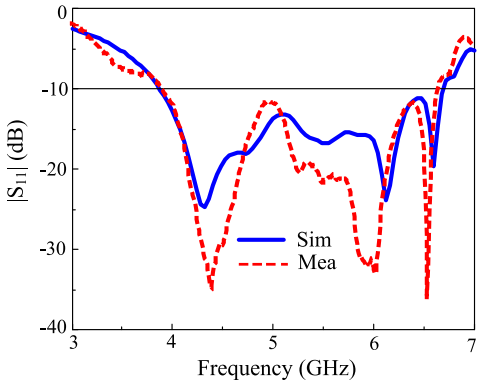

FIGURE 12. Measured and simulated reflection coefficient values.

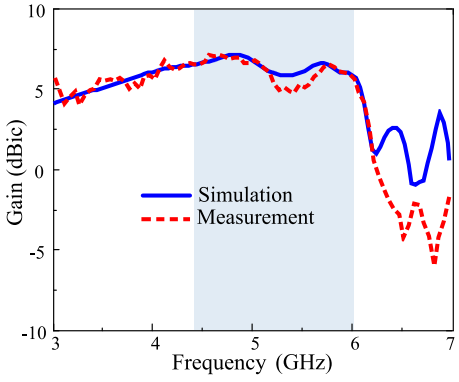

FIGURE 13. Measured and simulated gain.

x-*z* and *y*-*z* planes for both RHCP (i.e., co-polarization) and LHCP (i.e., cross-polarization) at 5.1 GHz are presented in Fig. 15.

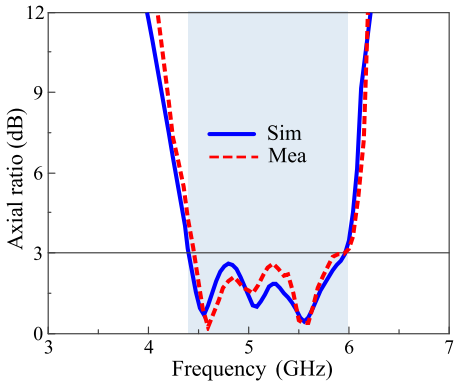

FIGURE 14. Measured and simulated axial ratio.

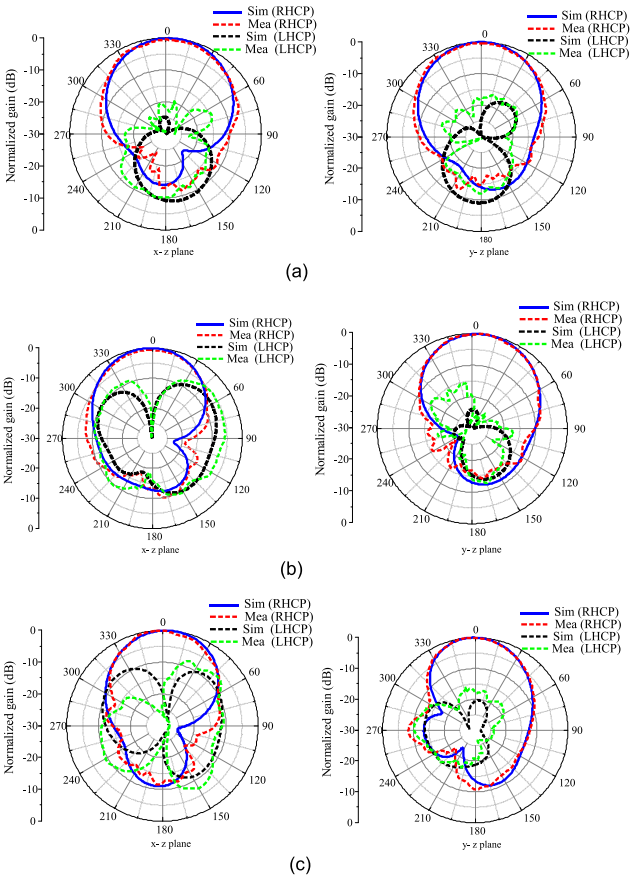

FIGURE 15. Simulated and measured RHCP (co-polarized) and LHCP (cross-polarized) at (a) 4.6 GHz, (b) 5.1 GHz, and (c) 5.6 GHz.

IV. EXPERIMENTAL RESULTS

For verification, the proposed wideband metasurface-based antenna was fabricated and measured. Fig. 11 shows the fabricated sample of the prototype. For S-parameter measurements, an Agilent N5230A network analyzer and a 3.5-mm coaxial calibration standard GCS35M were employed. Far-field measurements were conducted at the RFID/USN Center, Incheon, in the Republic of Korea. For radiation pattern measurements, a full anechoic chamber and an

TABLE 1. Performance comparison of the proposed antenna with other antenna designs.

Antenna structure	Size (λ_o^3)	−10 dB BW (%)	AR. BW (%)	Peak gain (dBic)	Center Freq. (GHz)
Ref. [15]	0.98 × 0.98× 0.06	15.5	8	5.8	2.45
Ref. [17]	0.58× 0.58 × 0.04	22	8.6	6.5	3.5
Ref. [18]	0.67 × 0.67 × 0.065	39.25	17.7 7	6.5	5.5
Ref. [19]	0.79 × 0.79 × 0.067	20.6	17.4	8.2	5.5
Ref. [20]	0.075 × 0.073 × 0.086	32.1	20	7.9	5.5
Ref. [21]	0.66 × 0.66 × 0.078	43.3	22	6.16	5.9
Proposed	0.71 × 0.71 × 0.038	55.7	31.3 7	7	5.1

λ_o: the free-space wavelength corresponding to the center frequency of the AR bandwidth.

Agilent E8362B network analyzer were employed. The proposed wideband metasurface-based antenna was used for reception, and a standard wideband horn antenna was used for transmission. The transmission distance of 10 m was established between the antennas to satisfy the far-field condition. The proposed antenna was rotated from –180° to 180° at 3°/s and a 1° scan angle while the horn antenna remained fixed. Overall, the results of the proposed antenna show good agreement between the simulated and measured data. There exist minimal disparities between the measurements and the HFSS simulations, and this may be due to the slight alignment errors during fabrication. Fig. 12 shows the measured and simulated reflection coefficients for the fabricated antenna. The measured impedance bandwidth for $|S_{11}| < -10$ dB is 3.75–6.7 GHz (56.7%), which is similar to the simulated impedance bandwidth of 3.75–6.67 GHz (55.7%).

Fig. 13 shows the measured and simulated gains for the proposed antenna with a simulated peak gain of 7.15 dBic and a measured peak gain of 7 dBic at the broadside direction for (phi = 0°) and (theta = 0°). The AR and radiation patterns of the fabricated prototype (at 4.6 GHz, 5.1 GHz, and 5.6 GHz) were measured and are shown in Figs. 14 and 15, respectively. Fig. 14 shows the measured and simulated AR bandwidth of the proposed antenna. The simulated AR bandwidth is 4.36–5.98 GHz (31.76%), and the measured AR bandwidth is 4.38–5.98 GHz (31.37%). The measured and simulated radiation patterns are shown in Fig. 15. As shown in Figs. 15 (a), (b), and (c), respectively, the measured and simulated radiation patterns at 4.6 GHz, 5.1 GHz, and 5.6 GHz show good symmetrical RHCP and low cross-polarization.

Table 1 compares the performance of the proposed antenna with that of other unidirectional antenna designs described in the literature. The selection criteria of the [15] and [17]–[21] comparison tables was based on comparing our design's size, impedance bandwidth, AR bandwidth, and gain to previous state of arts which used single radiating element LP source and an LP to CP polarization conversion metasurfaces which was stacked above the radiator. Our proposed antenna shows a wide impedance bandwidth, wide 3-dB AR bandwidth, and low profile compared with the other aforementioned antennas [15], [17]–[21].

V. CONCLUSION

In this paper, a low-profile wideband CP antenna is presented. The low-profile wideband antenna consists of the metasurface made of 4 ×4 corner-truncated patches placed on top of the antenna, and a bowtie-shaped slot etched on the ground plane placed at the bottom of the antenna. The corner-truncated metasurface patches are used for the conversion of LP to CP radiation. The proposed antenna has a compact structure with a low profile of 0.038 λ_o. The measured results show that the antenna has an impedance bandwidth of 3.75–6.67 GHz (55.7%), an AR bandwidth of 4.38– 5.98 GHz (31.37%), a 3-dB gain bandwidth of 3.75–6.0 GHz (46.88%), a peak gain of 7 dBic, and a high radiation efficiency of over 93%. Because of its low profile and compact structure, wide impedance bandwidth, and wide axial ratio bandwidth, the proposed antenna is suitable for C-band satellite communication.

REFERENCES

[1] D. Sievenpiper, L. Zhang, R. F. J. Broas, N. G. Alexopolous, and E. Yablonovitch, "High-impedance electromagnetic surfaces with a forbidden frequency band," *IEEE Trans. Microw. Theory Techn.*, vol. 47, no. 11, pp. 2059–2074, Nov. 1999.

[2] M. Hosseini and M. Hakkak, "Characteristics estimation for Jerusalem cross-based artificial magnetic conductors," *IEEE Antennas Wireless Propag. Lett.*, vol. 7, pp. 56–61, 2008.

[3] F. Yang and Y. Rahmat-Samii, "Mutual coupling reduction of microstrip antennas using electromagnetic band-gap structure," in *IEEE AP-S Dig.*, Jul. 2000, pp. 674–677.

[4] W. Liu, Z. N. Chen, and X. Qing, "Metamaterial-based low-profile broadband mushroom antenna," *IEEE Trans. Antennas Propag.*, vol. 62, no. 3, pp. 1165–1172, Mar. 2014.

[5] W. Liu, Z. N. Chen, and X. Qing, "Metamaterial-based low-profile broadband aperture-coupled grid-slotted patch antenna," *IEEE Trans. Antennas Propag.*, vol. 63, no. 7, pp. 3325–3329, Jul. 2015.

[6] F. H. Lin and Z. N. Chen, "Low-profile wideband metasurface antennas using characteristic mode analysis," *IEEE Trans. Antennas Propag.*, vol. 65, no. 4, pp. 1706–1713, Apr. 2017.

[7] D. Chen, W. Yang, Q. Xue, and W. Che, "Miniaturized wideband planar antenna using interembedded metasurface structure," *IEEE Trans. Antennas Propag.*, vol. 69, no. 5, pp. 3021–3026, May 2021.

[8] F. A. Diana and S. Genovesi, "Characteristic modes analysis of non-uniform metasurface superstrate for nanosatellite antenna design," *IEEE Access*, vol. 8, pp. 1053–1058, 2020.

[9] I. Park, "Application of metasurfaces in the design of performance-enhanced low-profile antennas," *EPJ Appl. Metamater.*, vol. 5, no. 11, pp. 1–12, Nov. 2018.

[10] D. Chen, W. Yang, W. Che, and Q. Xue, "Broadband stable-gain multiresonance antenna using nonperiodic square-ring metasurface," *IEEE Antennas Wireless Propag. Lett.*, vol. 18, no. 8, pp. 1537–1541, Aug. 2019.

[11] J. Wang, H. Wong, Z. Ji, and Y. Wu, "Broadband CPW-fed aperture coupled metasurface antenna," *IEEE Antennas Wireless Propag. Lett.*, vol. 18, no. 3, pp. 517–520, Mar. 2019.

[12] W. E. I. Liu, Z. N. Chen, X. Qing, J. Shi, and F. H. Lin, "Miniaturized wideband metasurface antennas," *IEEE Trans. Antennas Propag.*, vol. 65, no. 12, pp. 7345–7349, Dec. 2017.

[13] S. X. Ta and I. Park, "Low-profile broadband circularly polarized patch antenna using metasurface," *IEEE Trans. Antennas Propag.*, vol. 63, no. 12, pp. 5929–5934, Dec. 2015.

[14] Z. Wu, L. Li, Y. Li, and X. Chen, "Metasurface superstrate antenna with wideband circular polarization for satellite communication application," *IEEE Antennas Wireless Propag. Lett.*, vol. 15, pp. 374–377, 2016.

[15] H. L. Zhu, S. W. Cheung, K. L. Chung, and T. I. Yuk, "Linear-to-circular polarization conversion using metasurface," *IEEE Trans. Antennas Propag.*, vol. 61, no. 9, pp. 4615–4623, Sep. 2013.

[16] H. L. Zhu, S. W. Cheung, X. H. Liu, and T. I. Yuk, "Design of polarization reconfigurable antenna using metasurface," *IEEE Trans. Antennas Propag.*, vol. 62, no. 6, pp. 2891–2898, Jun. 2014.

[17] Y. Juan, W. Yang, and W. Che, "Miniaturized low-profile circularly polarized metasurface antenna using capacitive loading," *IEEE Trans. Antennas Propag.*, vol. 67, no. 5, pp. 3527–3532, May 2019.

[18] J. Dong, C. Ding, and J. Mo, "A low-profile wideband Linear-to-Circular polarization conversion slot antenna using metasurface," *Materials*, vol. 13, no. 5, p. 1164, Mar. 2020.

[19] L. Yuan, H. Yu-Xuan, L. Zhan-Wei, C. Shu-Ting, X. Xiao-Ming, and G. Jing, "Design of a compact wideband CP metasurface antenna," *Int. J. RF Microw. Comput.-Aided Eng.*, vol. 30, no. 10, Oct. 2020, Art. no. e22332, doi: 10.1002/mmce.22332.

[20] Y. Huang, L. Yang, J. Li, Y. Wang, and G. Wen, "Polarization conversion of metasurface for the application of wide band low-profile circular polarization slot antenna," *Appl. Phys. Lett.*, vol. 109, no. 5, pp. 1–5, 2016.

[21] N. Supreeyatitikul, T. Lertwiriyaprapa, and C. Phongcharoenpanich, "S-shaped metasurface-based wideband circularly polarized patch antenna for C-band applications," *IEEE Access*, vol. 9, pp. 23944–23955, 2021.

[22] Q. Zheng, C. Guo, and J. Ding, "Wideband and low RCS planar circularly polarized array based on polarization conversion of metasurface," *Microw. Opt. Technol. Lett.*, vol. 60, no. 3, pp. 784–789, Mar. 2018.

[23] K. Li, Y. Liu, Y. Jia, and Y. J. Guo, "A circularly polarized high-gain antenna with low RCS over a wideband using chessboard polarization conversion metasurfaces," *IEEE Trans. Antennas Propag.*, vol. 65, no. 8, pp. 4288–4292, Aug. 2017.

[24] S. X. Ta and I. Park, "Planar wideband circularly polarized metasurface-based antenna array," *J. Electromagn. Waves Appl.*, vol. 30, no. 12, pp. 1620–1630, 2016.

[25] C. H. S. Nkimbeng, H. Wang, and I. Park, "Coplanar waveguide-fed bidirectional same-sense circularly polarized metasurface-based antenna," *J. Electromagn. Eng. Sci.*, vol. 21, no. 3, pp. 210–217, Jul. 2021.

[26] Q. W. Lin, H. Wong, X. Y. Zhang, and H. W. Lai, "Printed meandering probe-fed circularly polarized patch antenna with wide bandwidth," *IEEE Antennas Wireless Propag. Lett.*, vol. 13, pp. 654–657, 2014.

[27] M. Ameen, O. Ahmad, and R. K. Chaudhary, "Wideband circularly-polarised high-gain diversity antenna loaded with metasurface reflector for small satellite applications," *Electron. Lett.*, vol. 55, no. 15, pp. 829–831, Jul. 2019.

[28] S. X. Ta and I. Park, "Compact wideband circularly polarized patch antenna array using metasurface," *IEEE Antennas Wireless Propag. Lett.*, vol. 16, pp. 1932–1936, 2017.

[29] X. Zhang and L. Zhu, "High-gain circularly polarized microstrip patch antenna with loading of shorting pins," *IEEE Trans. Antennas Propag.*, vol. 64, no. 6, pp. 2172–2178, Jun. 2016.

[30] C. L. Holloway, E. F. Kuester, J. A. Gordon, J. O'Hara, J. Booth, and D. R. Smith, "An overview of the theory and applications of metasurfaces: The two-dimensional equivalents of metamaterials," *IEEE Antenn. Propag. Mag.*, vol. 54, no. 4, pp. 10–35, Apr. 2012.

[31] Y. Jia, Y. Liu, and S. Gong, "Wideband high-gain circularly polarized planar antenna based on polarization rotator," in *Proc. Int. Conf. Electromagn. Adv. Appl. (ICEAA)*, Cairns, QLD, Australia, Sep. 2016, pp. 416–419.

[32] J. Y. Chin, M. Lu, and T. J. Cui, "Metamaterial polarizers by electric-field-coupled resonators," *Appl. Phys. Lett.*, vol. 93, no. 25, Dec. 2008, Art. no. 251903, doi: 10.1063/1.3054161.

[33] E. A. Soliman, S. Brebels, P. Delmotte, G. A. E. Vandenbosch, and E. Beyne, "Bow-tie slot antenna fed by CPW," *Electron. Lett.*, vol. 35, no. 7, pp. 514–515, 1999.

[34] M. Miao, B. L. Ooi, and P. S. Kooi, "Broadband CPW-fed wide slot antenna," *Microw. Opt. Technol. Lett.*, vol. 25, no. 3, pp. 206–211, May 2000.

[35] L. Marantis and P. Brennan, "A CPW-fed bow-tie slot antenna with tuning stub," in *Proc. Loughborough Antennas Propag. Conf.*, Mar. 2008, pp. 389–392, doi: 10.1109/LAPC.2008.4516948.

[36] M. Naser-Moghadasi, A. Danideh, R. Sadeghifakhr, and M. Reza-Azadi, "CPW-fed ultra wideband slot antenna with arc-shaped stub," *IET Microw., Antennas Propag.*, vol. 3, no. 4, pp. 681–686, 2009, doi: 10.1049/iet-map.2008.0057.

[37] C.-Y. Huang and D.-Y. Lin, "CPW-fed bow-tie slot antenna for ultra-wideband communications," *Electron. Lett.*, vol. 42, no. 19, pp. 1073–1074, 2006.

[38] M. A. Riheen, T. T. Nguyen, T. K. Saha, T. Karacolak, and P. K. Sekhar, "CPW fed wideband bowtie slot antenna on PET substrate," *Prog. Electromagn. Res.*, vol. 101, pp. 147–158, 2020.

[39] T. Kamei, Y. Utsumi, N. Q. Dinh, and N. Thanh, "Wide-band coaxial-to-coplanar transition," *IEICE Trans. Electron.*, vol. E90-C, no. 10, pp. 2030–2036, Oct. 2007.

[40] N. Haider, D. Caratelli, D. P. Tran, and A. G. Yarovoy, "Directive electric–magnetic antenna for ultra-wideband applications," *IET Microw., Antennas Propag.*, vol. 7, no. 5, pp. 381–390, Apr. 2013, doi: 10.1049/iet-map.2012.0494.

[41] D. P. Tran, F. M. Tanyer-Tigrek, I. E. Lager, and L. P. Ligthart, "A novel unidirectional radiator with superb UWB characteristics for X-band phased array applications," in *Proc. Eur. Conf. Antennas Propag.*, Berlin, Germany, Mar. 2009, pp. 1617–1621.

[42] C. Ni, C. Liu, Z. Zhang, M. Chen, L. Zhang, and X. Wu, "Design of broadband high gain polarization reconfigurable Fabry–Pérot cavity antenna using metasurface," *Frontiers Phys.*, vol. 8, pp. 1–9, Aug. 2020, doi: 10.3389/fphy.2020.00316.

[43] C. Ni, M. S. Chen, Z. X. Zhang, and X. L. Wu, "Design of frequency- and polarization-reconfigurable antenna based on the polarization conversion metasurface," *IEEE Antennas Wireless Propag. Lett.*, vol. 17, no. 1, pp. 78–81, Jan. 2018.

[44] M. U. Afzal, A. Lalbakhsh, and K. P. Esselle, "Method to enhance directional propagation of circularly polarized antennas by making near-electric field phase more uniform," *IEEE Trans. Antennas Propag.*, vol. 69, no. 8, pp. 4447–4456, Aug. 2021.

CHO HILARY SCOTT NKIMBENG received the B.Tech. degree in electrical and electronic engineering (telecommunication) from the University of Buea, Cameroon, in 2013, and the M.S. degree in electrical and computer engineering from Ajou University, Suwon-si, Republic of Korea, in 2018, where he is currently pursuing the Ph.D. degree with the Department of Electrical and Computer Engineering. His research interests include metasurface antennas, metamaterial-based antennas, circularly polarized antennas, miniaturized antennas, and bidirectional antennas.

HEESU WANG (Graduate Student Member, IEEE) received the B.S. and M.S. degrees in electrical and computer engineering from Ajou University, Suwon-si, Republic of Korea, in 2018 and 2020, respectively, where he is currently pursuing the Ph.D. degree with the Department of Electrical and Computer Engineering. His research interests include the design of patch antennas, printed antennas, small antennas, and metasurface antennas for various wireless communication applications.

IKMO PARK (Member, IEEE) received the B.S. degree in electrical engineering from the State University of New York at Stony Brook and the M.S. and Ph.D. degrees in electrical engineering from the University of Illinois at Urbana-Champaign.

He joined the Department of Electrical and Computer Engineering, Ajou University, in 1996. Prior to joining Ajou University, he has been working with the Device & Materials Laboratory, LG Corporate Institute of Technology, Seoul, Republic of Korea, where he had been engaged in research and development of various antennas for personal communication systems, wireless local area networks, and direct broadcasting systems. He was a Visiting Professor at the Department of Electrical and Computer Engineering, POSTECH, Pohang-si, Republic of Korea, from March 2004 to February 2005, and the Department of Electrical and Computer Engineering, The University of Arizona, Tucson, AZ, USA, from July 2011 to June 2012. He served as the Chair of the Department of Electrical and Computer Engineering, Ajou University. He has authored and coauthored over 350 technical journals and conference papers. He also holds over 50 domestic and international patents. His current research interests include the design and analysis of microwave, millimeter-wave, terahertz wave, and nano-structured antennas.

Prof. Park served as an Editorial Board Member of the *Journal of Electromagnetic Engineering and Science*. He is a member of the Board of Directors of Korea Institute of Electromagnetic Engineering and Science (KIEES), an Editorial Board Member of the *International Journal of Antennas and Propagation*, and a member of Eta Kappa Nu and Tau Beta Pi. He was a recipient of several awards and recognitions, including the KIEES Outstanding Scholarly Achievement Award, in 2014, the KIEES Outstanding Researcher Award, in 2013, the KIEES Distinguished Service Award, in 2012, the KIEES Meritorious Award, in 2015, the Ajou Publication Award, in 2013, the Ajou Dasan Research Award, in 2017 and 2018, the Distinguished Service Award from the Department of Electrical and Computer Engineering, Ajou University, in 2011, the Outstanding Advisor Award from the Radio Engineering and Research Center, KAIST, in 2009, the Best Paper Award from Optical Society of Korea (OSK), in 2007, the Best Paper Award from KIEES, in 2010 and 2016, the IEEE iWAT Best Poster Paper Award, in 2005, and the Haedong Best Paper Award from the Institute of Electronics Engineers of Korea (IEEK), in 2002. He serves as the chair, an organizer, and a member of the program committees for various conferences, workshops, and short courses in electromagnetic related topics. He is also a frequent reviewer of over ten scientific journals and book publishers. He serves as the Editor-in-Chief of *The Proceeding of the KIEES* and journal of *KIEES*, and an Associate Editor for *IET Electronics Letters*.